Multiscale and Multidisciplinary Modeling, Experiments and Design (2019) 2:249–258
https://doi.org/10.1007/s41939-019-00051-4

ORIGINAL PAPER

A simplified constitutive and finite element model of plain weave fabric reinforcements for the biaxial loading

Munshi M. Basit[1] · Shen-Yi Luo[2] · Aniruddha Mitra[1]

Received: 12 April 2019 / Accepted: 23 May 2019 / Published online: 4 June 2019

Abstract
Soft matrices reinforced by textile preforms are considered as flexible composites that can undergo large elastic deformation. The mechanical behaviors of these composites are highly nonlinear, involving both material and geometric nonlinearities. To conduct a finite element analysis studying woven fabric structures, one of the desired approaches is to develop an equivalent continuum model representing the mechanical behavior of the fabric's unit cell. During large deformation, significant fabric architecture rearrangement occurs. To include this geometrical nonlinearity into a continuum model, it is always a challenge. In this work, the constitutive model of weave fabrics under biaxial loadings has been derived considering the large nonlinear elastic deformations. This model assumes that the fabric consists of monofilaments, where the yarn is treated as a thin isotropic solid bar which follows the sinusoidal shape. The effects of the yarn's crimp interchange, and bending are considered in the constitutive equations. One of the special advantages to use this constitutive model is that the geometry can be completely defined by the commonly given information for a fabric (i.e., crimps, number of yarns per unit fabric length). Good agreement has been found between predictions and experiments under various biaxial loadings. The theoretical predictions also agree well with FEA simulations of the mechanical behaviors of the unit cell.

Keywords Plain weave fabrics · Textile composite · Biaxial loading · Finite element analysis (FEA) · Analytical modeling

1 Introduction

Researchers and engineers prefer textile composites due to their superior mechanical and chemical properties, e.g., high specific stiffness and strength, dimensional stability, low thermal expansion, and good corrosion resistance. Most important is that textile composites are more flexible than all continuous material; therefore, they are particularly suitable for manufacturing components with complex shape. Along with these advantages, composite materials based on woven fabric reinforcements achieve high stiffness and strength, comparable with traditional fiber reinforcements (Adumitroaie and Barbero 2012). Plain weave fabrics are chosen as a research topic since plain weave fabrics are widely used as reinforcements in textile composites. Plain weave fabric reinforcements are widely employed in aircraft, boats and pressure vessels, because they can provide more balanced properties than a unidirectional laminate. In the last decade, there has been an increasing trend in the application of flexible dry woven fabrics in various fields spanning from personal protective garments to composite materials. They can offer a superior combination of properties such as high tenacity, strength-to-weight ratios and flexibility (Erol et al. 2017). Moreover, due to the flexibility plain weave reinforce composite are widely used in curvature type structure (Boisse et al. 2006; Launay et al. 2008). The fabrication cost of flexible composite reinforced by plain weave fabric is comparatively low. Since the cost of plain weave fabric composite fabrication is cheap, easy to handle and have many advantages as discussed above; it is important to study the mechanical behavior of such fabrics to fully realize their potential to be used as composite reinforcement (Barbero et al. 2006a).

In this study, biaxial loading is considered to characterize the mechanical behavior of plain weave fabric. Since, plain weave fabric reinforce composite suffers biaxial loading condition in many practical case, however

✉ Munshi M. Basit
mbasit@georgiasouthern.edu

[1] Department of Mechanical Engineering, Georgia Southern University, Statesboro, USA

[2] Department of Mechanical Engineering, University of Nevada, Reno, USA

biaxial experimental setup is expensive and often fails to obtain fully reliable data due to the architectural nonlinearity of the fabric specimen. Biaxial data are needed both for investigating the stress–strain behavior of orthotropic composites used in structural applications as well as for assessing the reliability of failure criteria (Barbero et al. 2006b; Boehler et al. 1994; Welsh and Adams 2002; Zhang and Harding 1990). From the literature (Ito and Chou 1998; Adumitroaie and Barbero 2012; Naik 1995; Buet-Gautier and Boisse 2001), it could be concluded that one of the most frequent concerns associated with the use of modern composite materials and textiles is the inability of researchers to accurately model the onset of failure under complex biaxial loading conditions and a universally accepted failure theory for unidirectional composite materials has not been developed yet mainly due to the lack of reliable biaxial experimental data.

Therefore, finite element models and theoretical analysis could solve the problem of verifying experimental data. Many studies have been conducted before to characterize the mechanical behavior of plain weave fabric during biaxial loading (El-Messiry and Youssef 2011; Pan 1996; Kumazawa et al. 2005; Gasser et al. 2000) and shear loading (Basit and Luo 2018; Sun and Pan 2005; Mohammed et al. 2000; Daelemans et al. 2016; Page and Wang 2000; Cao et al. 2008). In this study, a simplified biaxial constitutive model has been proposed that needs only the common information of fabric as the input. Moreover, a finite element analysis was conducted. To conduct a finite element analysis on plain weave fabric structures, one of the desired approaches is to develop an equivalent continuum model representing the mechanical behavior of the fabric's unit cell. Experiments show that, during large deformation, the fabric architecture may change significantly (e.g., crimp interchange). The fiber reorientation affects the mechanical behavior of the unit cell, and causes geometrical nonlinearity. To include the geometrical nonlinearity into a general continuum model is always a challenge.

A comprehensive experimental study of plain weave fabrics under various ratios of biaxial loading was reported in reference (Freeston et al. 1967). Since sufficient information is provided, these experimental results are used as an example in the comparison study. The experimental engineering stress–strain curves of a plain weave fabric under various biaxial loadings (Freeston et al. 1967) are shown in Fig. 1, whereas nomenclature are listed in Table 1. When the fabric is under loading N_x:N_y = 1:1, the pattern is similar to a linear orthotropic composite laminate. While, under loading N_x:N_y = 5:1, the strain (solid triangle) in the minor load direction tends to go negative first before moving to the positive direction. This indicates that the internal fabric architecture rearrangement not only depends on the magnitude of the loading, but also the path and ratio.

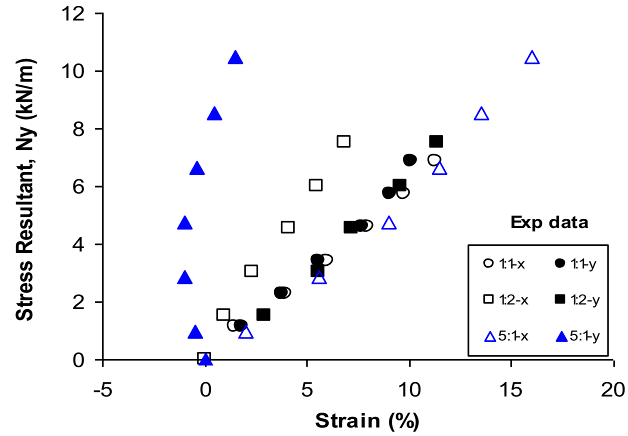

Fig. 1 Experimental results of undyed saran monofilaments fabric under biaxial loading, N_x:N_y = 1:1, 1:2, 5:1

The objective of this work is to develop an equivalent continuum model for plain weave fabric under biaxial loading. The sinusoidal unit cell model, used in this work, describes the overall mechanical behavior of the fabrics (i.e., the biaxial stress resultant and fabric strain). The required inputs are (1) initial crimps, (2) number of yarns per unit fabric length, and (3) yarn properties. The predictions from the current model agree with the experimental data (Freeston et al. 1967) for a fabric under biaxial loading of 0:1, 1:1, 1:2, 1:5 and 5:1. They also agree well with FEA simulations of the mechanical behaviors of the unit cell.

2 Geometry of a unit cell

A unit cell of a plain weave fabric with initial in-plane dimensions of L_{x0} and L_{y0} is shown in Fig. 2. The unit cell was first proposed by (Kawabata et al. 1973) to study the biaxial properties of woven fabric. Two curved filling yarns and two curved warp yarns are interlaced over and under one another. Let the filling and warp yarns be denoted by x and y, respectively.

Let z_ξ be the coordinate of the ξ-yarn ($\xi = x$ or y) along the thickness direction; $a_{\xi 0}$ and $L_{\xi 0}$ the initial amplitude and wavelength of the sinusoidal curve of ξ yarn, respectively, as shown in Fig. 2.

Referring to Fig. 2b, the positions of the yarns can be expressed as:

$$\begin{aligned} z_x &= a_{x0} \sin\left(\frac{2\pi x}{L_{x0}}\right) \\ z_y &= -a_{y0} \sin\left(\frac{2\pi y}{L_{y0}}\right). \end{aligned} \tag{1}$$

Crimp is the ratio of difference between straightened arc length, and wavelength to the wavelength. Crimp is

Table 1 Nomenclature

Definition	Symbol
x, or y	ξ
Total arc length of ξ-yarn in an undeformed unit cell	$S_{\xi 0}$
Total arc length of ξ-yarn in a deformed unit cell	S_{ξ}
Initial wavelength of the ξ-yarn wave	$L_{\xi 0}$
Current wavelength of the ξ-yarn wave after deformation	L_{ξ}
Amplitude of the ξ-yarn wave in a deformed unit cell	a_{ξ}
Initial amplitude of the ξ-yarn wave in an undeformed unit cell	$a_{\xi 0}$
Crimp of the ξ-yarn or $(S_{\xi 0}/L_{\xi 0} - 1)$	$\text{Crimp}_{-\xi}$
Number of the ξ-yarns per unit length of fabric	n_{ξ}
Distance between ξ-yarn center and its surface along z direction	r_{ξ}
Rigid body displacement of the contact point	δ
Normal strain of the unit cell in the ξ direction	ε_{ξ}
Yarn's axial strain	$\varepsilon_{f-\xi}$
Stress resultant (normal force per unit length of the fabric) in ξ direction	N_{ξ}
Effective Poisson's ratio of the yarn	ν
Cross-sectional area of the circular yarn	A
Strain energy stored in a unit cell	U
Energy stored in a ξ-yarn due to the yarn axial strain	$u_{f-\xi}$
Energy stored in a ξ-yarn due to the lateral displacement	$u_{b-\xi}$
Shear modulus of the yarn referring to the longitudinal-transverse plane	$G_{z\xi}$
Lateral stiffness of a half of a yarn	k_{ξ}

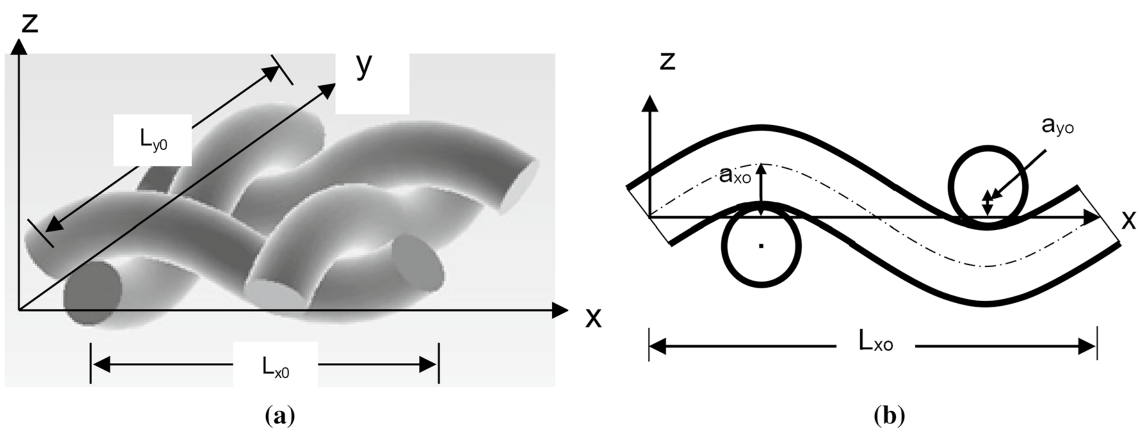

Fig. 2 **a** Unit cell of a plain woven fabric with wavelengths ($L_{\xi 0}$, where ξ is either x or y); **b** cross-section along an x-yarn

the measure of waviness of a fabric. For a fabric, crimps (crimp_{-x} and (crimp_{-y}), and the number of yarns per unit fabric length (n_x and n_y) are usually given in the datasheet, or can be easily measured. Referring to Fig. 2 and from the definition of crimp, the wavelength (L_{x0} and L_{y0}) and arc length (S_{x0} and S_{y0}) of the undeformed yarns can be calculated as:

$$
\begin{aligned}
&L_{x0} = 2/n_y, \quad L_{y0} = 2/n_x \\
&S_{x0} = L_{x0}(1 + \text{crimp}_{-x}), \quad S_{y0} = L_{y0}(1 + \text{crimp}_{-y}),
\end{aligned}
\tag{2}
$$

where $\text{crimp}_{-\xi}$ is the crimp of the ξ-yarn; and n_{ξ} is the number of ξ-yarns per unit fabric length of the fabric along its perpendicular direction.

Referring to Fig. 3, the yarn's arc length ($S_{\xi 0}$) in an undeformed fabric unit cell can be mathematically expressed as (Luo and Mitra 1999):

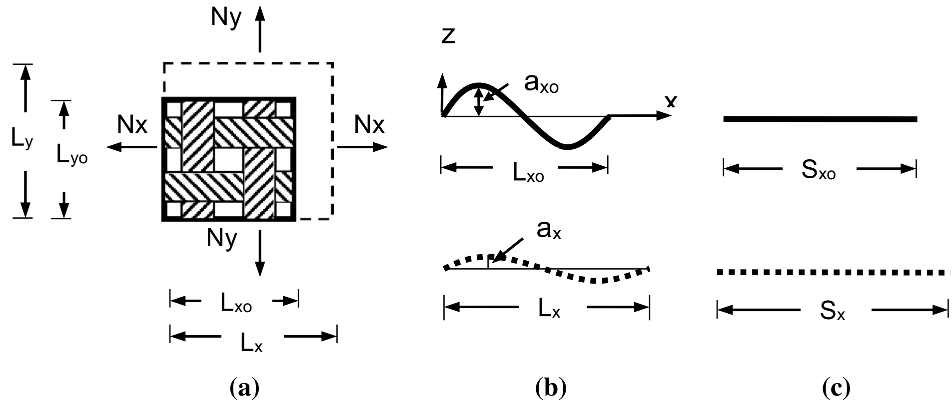

Fig. 3 **a** Biaxial deformation of a unit cell; **b** wavelength and arc length of an x-yarn in undeformed unit cell; **c** wavelength and arc length of an x-yarn in deformed unit cell

$$\begin{aligned} S_{x0} &= \int_0^{L_{x0}} \sqrt{1 + \left(\frac{2\pi a_{x0}}{L_{x0}}\right)^2 \cos^2\left(\frac{2\pi x}{L_{x0}}\right)} \mathrm{d}(x) \\ S_{y0} &= \int_0^{L_{y0}} \sqrt{1 + \left(\frac{2\pi a_{y0}}{L_{y0}}\right)^2 \cos^2\left(\frac{2\pi y}{L_{y0}}\right)} \mathrm{d}(y). \end{aligned} \tag{3}$$

The geometry of the fabric sinusoidal model can be completely defined by Eqs. (1)–(3) with commonly given information (i.e., crimps, n_ξ).

2.1 Input information

The material properties and fabric information are recaptured from Page and Wang (2000) as the following:

Number of yarns per inch fabric length (filling), $n_x = 33.25$
Number of yarns per inch fabric length (warp), $n_y = 31.5$
Filling yarn crimp$_{-x} = 2.75\%$
Warp yarn crimp$_{-y} = 5.5\%$
Yarn modulus $E_f = 145$ ksi (approximately linear)
Yarn diameter $d = 10.2 \times 10^{-3}$ in

Calculated fabric properties and initial geometric parameters are listed in Table 2. First L_{x0}, L_{y0}, S_{x0}, and S_{y0} were calculated from input information and using Eq. (2). Then a_{x0}, a_{y0} were calculated using equation number (3). Cross-sectional area of the yarns was calculated from the yarn diameter assuming they have circular cross-section. The cross-section of yarn is often represented by oval, elliptical, lens or circular shape. For simplicity, the geometry of the unit cell has been described by assuming that both the yarn cross-section and the undulated length can by represented by arcs of circles (Afrashteh et al. 2013; Behera et al. 2012). It was reported that the yarn cross-section partially returns to its circular shape with the release of pressure on it, whether the twist factor is high or low (Ozgen and Gong 2010).

3 Biaxial deformation of a unit cell

If a fabric is treated as a continuum, the biaxial loading and deformation are illustrated in Fig. 3a. The stress resultants N_x and N_y are defined as the tensile force per unit length of the fabric; the engineering strains of the fabric:

$$\begin{aligned} \varepsilon_x &= \frac{\Delta L_x}{L_{x0}} = \frac{L_x - L_{x0}}{L_{x0}}, \\ \varepsilon_y &= \frac{\Delta L_y}{L_{y0}} = \frac{L_y - L_{y0}}{L_{y0}}, \end{aligned} \tag{4}$$

where L_x and L_y are the current dimensions of the deformed unit cell; and are also the current wavelengths of the deformed yarns. Due to the waviness, the axial strain of a yarn differs from the strain of the fabric as demonstrated by Fig. 3b, c. The average values of yarn's axial strain are

$$\begin{aligned} \varepsilon_{f-x} &= \frac{\Delta S_x}{S_{x0}} = \frac{S_x - S_{x0}}{S_{x0}}, \\ \varepsilon_{f-y} &= \frac{\Delta S_y}{S_{y0}} = \frac{S_y - S_{y0}}{S_{y0}}, \end{aligned} \tag{5}$$

where S_ξ is the current arc length of the ξ-yarn in a deformed unit cell (Fig. 3c). Similar to Eq. (3), S_ξ can be expressed in terms of the wavelengths L_ξ and current yarn amplitude a_ξ:

Table 2 Yarn properties and initial geometric parameters (before loading)

L_{x0} (mm)	L_{y0} (mm)	S_{x0} (mm)	S_{y0} (mm)	a_{x0} (mm)	a_{y0} (mm)	E (N/mm^2)	ν	EI (N-mm^2)	EA (N)
1.613	1.529	1.657	1.612	0.086	0.116	1000	0.35	0.221	52.70

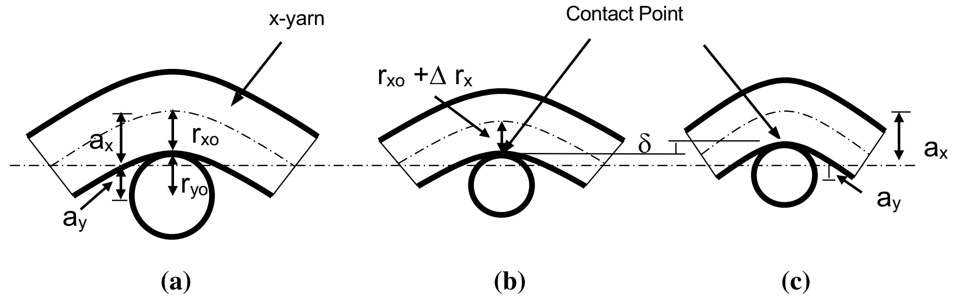

Fig. 4 **a** The undeformed amplitude; amplitude change of the wave of a yarn central line due to **b** flattening, $\varepsilon_{z\xi}$, and **c** rigid body displacement

$$S_x = \int_0^{L_x} \sqrt{1 + \left(\frac{2\pi a_x}{L_x}\right)^2 \cos^2\left(2\pi\left(\frac{x}{L_x}\right)\right)} \mathrm{d}(x),$$
$$S_y = \int_0^{L_y} \sqrt{1 + \left(\frac{2\pi a_y}{L_y}\right)^2 \cos^2\left(2\pi\left(\frac{y}{L_y}\right)\right)} \mathrm{d}(y). \tag{6}$$

Significant portion of the strain energy stored in the deformed fabric is due to the yarn axial extensions (or $S_\xi - S_{\xi 0}$). To determine S_ξ in a deformed fabric, a_ξ must be solved. As demonstrated in Fig. 4, the change of the yarn amplitudes is due to two factors:

1. The amount of distance change of r_ξ in the z (thickness) direction, Δr_ξ. r_ξ is the distance between the ξ-yarn's center and the contact point at the crossovers.
2. The lateral displacement (along z direction) of the contact point between warp and filling yarns δ.

The current amplitudes of the yarn centerline waves may be expressed as:

$$a_x = a_{x0} + \Delta r_x + \delta,$$
$$a_y = a_{y0} + \Delta r_y - \delta. \tag{7}$$

Notice that, in general, the yarn cross-section may have an ellipse shape, and $r_{\xi 0}$ should be measured from the fabric. For single-filament circular yarns, $r_{\xi 0}$ is the radius; and the yarn-flattening phenomenon is insignificant. The change in r_ξ is mainly contributed by the Poisson's ratio (ν) effect. For the problems with loading N_x and N_y as the inputs, we have:

$$\Delta r_x = -\nu \frac{\sigma_x}{E} r_{x0} = -\nu \frac{N_x L_{y0}}{2\mathrm{EA}} r_{x0},$$
$$\Delta r_y = -\nu \frac{\sigma_y}{E} r_{y0} = -\nu \frac{N_y L_{x0}}{2\mathrm{EA}} r_{y0}. \tag{8}$$

If the deformations (L_x and L_y) are the inputs, the change in r_ξ can be estimated as:

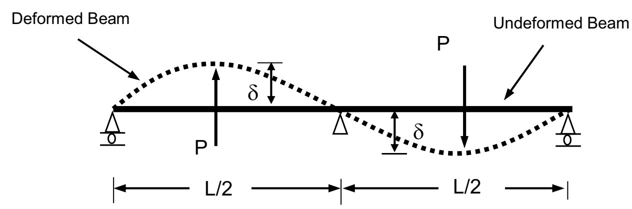

Fig. 5 Deflection of a straight yarn in unit cell

$$\Delta r_x = -\nu \varepsilon_{f-x} r_{x0},$$
$$\Delta r_y = -\nu \varepsilon_{f-y} r_{y0}, \tag{9}$$

where ε_{f-x} is the yarn's axial defined in Eq. (5).

δ is the vertical displacement of the contact point during fabric deformation. Fabric architecture rearrangements and crimp interchanges are mainly caused by this displacement. The value of δ depends on both the magnitude and ratio of the biaxial loading. Referring to Eqs. (4)–(7), the deformed unit cell is not only defined by the fabric overall strain, but also the lateral displacement δ. Thus, δ must be treated as an independent displacement variable into the constitutive equations developed in the following sections.

4 Strain energy and constitutive equation

For linear yarns, the axial tensile strain energy stored in a ξ -yarn of volume $AS_{\xi 0}$ can be expressed as:

$$u_{f-x} = \frac{1}{2}\mathrm{EA}S_{x0}\varepsilon_{f-x}^2,$$
$$u_{f-y} = \frac{1}{2}\mathrm{EA}S_{y0}\varepsilon_{f-y}^2, \tag{10}$$

where *EA* is the yarn axial stiffness, which can be obtained from yarn axial tensile tests.

To determine the bending energy, each half of the yarn is treated as a simply supported beam shown in Fig. 5. Due to biaxial loading, half of the yarn will undergo load in the upward direction, rest half downward, and vice versa. Then, the bending energy stored in a full ξ-yarn may be estimated as:

$$u_{b-x} = k_x \delta^2, \quad u_{b-y} = k_y \delta^2, \tag{11}$$

where k_ξ is the lateral stiffness of a half yarn simply supported as shown in Fig. 4. Applying classical shear beam theory, the value of the k_ξ can be estimated as:

$$\frac{1}{k_x} = \frac{L_{x0}^3}{384\mathrm{EI}} + \frac{L_{x0}}{8\mathrm{EA}}\frac{E}{G_{zx}}, \quad \frac{1}{k_y} = \frac{L_{y0}^3}{384\mathrm{EI}} + \frac{L_{y0}}{8\mathrm{EA}}\frac{E}{G_{zy}}, \tag{12}$$

where EI_f is the bending rigidity of the yarn. G is the shear modulus of the yarn referring to the longitudinal-transverse plane. There are two warp and two filling yarns in a unit cell, with Eqs. (10) and (11), the total strain energy stored in a unit cell is

$$U = \mathrm{EA}S_{x0}\varepsilon_{f-x}^2 + \mathrm{EA}S_{y0}\varepsilon_{f-y}^2 + 2K\delta^2, \quad K = k_x + k_y. \tag{13}$$

Based on the principal of virtual work, the constitutive equation of the plain weave fabrics under biaxial loading can be obtained as:

$$\begin{aligned} N_x &= \frac{1}{L_{y0}}\frac{\partial U}{\partial \Delta L_x} = \frac{2\mathrm{EA}}{L_{y0}}\varepsilon_{f-x}\frac{\partial S_x}{\partial L_x} \\ N_y &= \frac{1}{L_{x0}}\frac{\partial U}{\partial \Delta L_y} = \frac{2\mathrm{EA}}{L_{x0}}\varepsilon_{f-y}\frac{\partial S_y}{\partial L_y} \\ 0 &= \frac{\partial U}{\partial \delta} = 2\mathrm{EA}\varepsilon_{f-x}\frac{\partial S_x}{\partial \delta} + 2\mathrm{EA}\varepsilon_{f-y}\frac{\partial S_y}{\partial \delta} + K\delta. \end{aligned} \tag{14}$$

Equation (14) is the constitutive equation for a plain weave fabric under biaxial loading. If external loads (N_x and N_y) are given, external deformations (L_x and L_y) can be calculated by solving Eqs. (6) and (14) simultaneously. Here, Mathcad software was used to solve these equations. After solving, engineering and fabric strain can be calculated using Eqs. (4), and (5), respectively. The zero value shown in Eq. (14-3) represents no external lateral force acting at the yarn contact points. This additional equation solves δ which directly affects the fabric crimp interchange. The contact force can be calculated from Eq. (15). Note that P_x and P_y have equal value in the contact point:

$$\begin{aligned} P_x &= \frac{1}{2}\frac{\partial U_x}{\partial \delta} = \frac{1}{2}\mathrm{EA}\varepsilon_{f-x}\frac{\partial S_x}{\partial \delta} + k_x\delta, \\ P_y &= \frac{1}{2}\frac{\partial U_y}{\partial \delta} = \frac{1}{2}\mathrm{EA}\varepsilon_{f-y}\frac{\partial S_y}{\partial \delta} + k_y\delta. \end{aligned} \tag{15}$$

5 Finite element model of biaxial loading

Quarter model of the unit cell was built in ANSYS. This model was built using fabric properties and initial geometric parameters listed in Table 2. Note that half of the length ($L_{\xi0}/2$) of yarn was being modeled to establish the quarter symmetry. The model was meshed with SOLID185 element. After meshing, it was carefully checked that whether any distortion of the element occurred. The element size was checked for convergence test. The whole analysis was run for different element sizes, and then the results were compared for those element sizes. The shape of the mesh was Hex/wedge.

The contact and target surfaces constitute a "Contact Pair" in ANSYS. In studying the contact between two bodies, the surface of one body is conventionally taken as a contact surface and the surface of the other body as a target surface. For a rigid–flexible contact, the contact surface is associated with the deformable body, and the target surface must be the rigid surface. For flexible–flexible contact, both contact and target surfaces are associated with deformable bodies. Therefore, flexible–flexible contact pair was chosen. Here, CONTA174 element type was used to create contact pair. CONTA174 is an 8-node element that is intended for general rigid–flexible and flexible–flexible contact analysis. Again, surface–surface contact pair option was used in this study.

5.1 Boundary condition

The input of this FE model was deformations (ΔL_x and ΔL_y) so that the resultant stress can be obtained from the solution. There are two different types of boundary conditions (symmetric and translational) which were applied on the area of the model as shown in Fig. 6. The boundary conditions applied on two ends of the yarns are shown in Fig. 6, described in the following:

$$B_{x-x} = \left(L_x - L_{x0}\right)/2, \tag{16a}$$

$$B_{z-x} = 0, \tag{16b}$$

$$B_{y-y} = \left(L_y - L_{y0}\right)/2, \tag{16c}$$

$$B_{z-y} = -2 \times ((a_x + a_y) - (a_{x0} + a_{y0})), \tag{16d}$$

where B represents the magnitude of displacement. First subscript stands for the direction of displacement (x, y or z); whereas the second for x- or y-yarn. The translational boundary condition along x and y directions were divided by 2 because half of the length ($L_{\xi0}/2$) of yarn was being modeled.

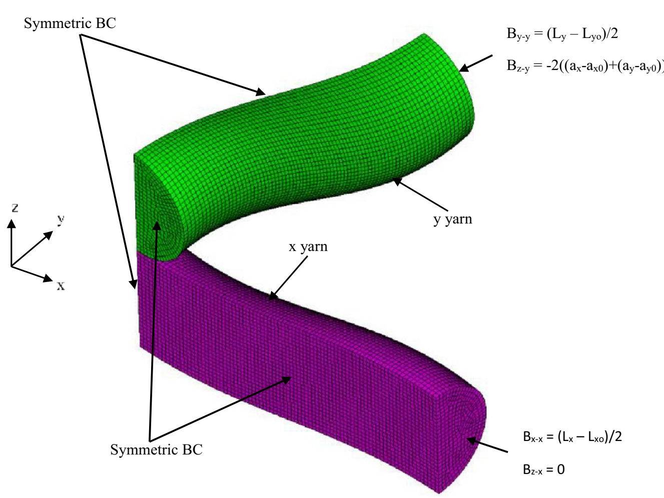

Fig. 6 Boundary condition on the sinusoidal model

5.2 Output

The input of the FE model was deformations (ΔL_x and ΔL_y) as mentioned in boundary condition. The output of FE model is reaction forces ($F_x/2$ and $F_y/2$) of master node shown in Fig. 7. Reaction force ($F_x/2$ and $F_y/2$) of master node was obtained from results of nodal solution after solving (nonlinear solution) the FE model by ANSYS. Note that the result of master node (shown in Fig. 7) represents the overall nodal results of corresponding nodes. Therefore, $F_x/2$ and $F_y/2$ are the load that exists in the end of the yarn model due to the applied deformation in the boundary condition. The resultant stress (N_x and N_y) was calculated from the ANSYS output (reaction load of $F_x/2$ and $F_y/2$), using following equations:

$$\begin{aligned} N_x &= 2\left(\frac{F_x}{2}\right)n_x, \\ N_y &= 2\left(\frac{F_y}{2}\right)n_y. \end{aligned} \tag{17}$$

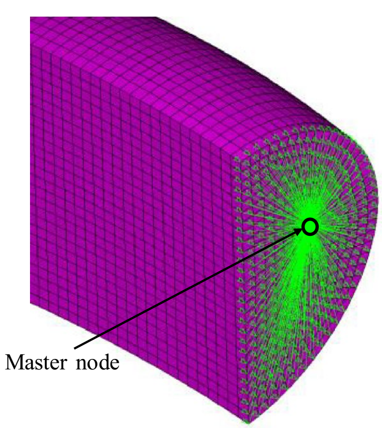

Fig. 7 Master node in the model of ANSYS

6 Biaxial model validation

6.1 Force–displacement

Comparisons have been made between the theoretical predictions and experimental results for the fabric under various biaxial loading ratios: N_x:N_y = 0:1, 1:5, 1:2, 1:1, and 5:1. The stress–strain relationship is presented in Fig. 8 for the loading ratio of N_x:N_y = 5:1. Figure 8 shows the experimental results verses predicted stress–strain curves calculated by analytical and FEA model for the fabric under biaxial loading of N_x:N_y = 5:1. The vertical axis is stress resultant defined as force per unit width of the fabric (kN/m). The horizontal axis is the engineering strain of the fabric. Note that only the values of major loading (N_x) are used to plot in

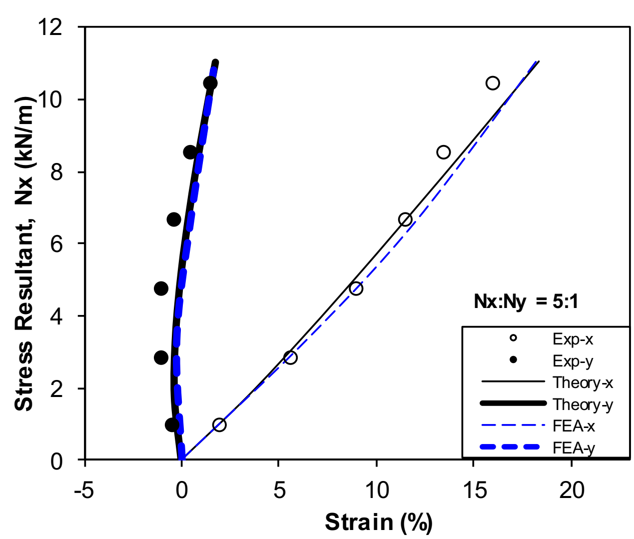

Fig. 8 Experimental data, theoretical and FEA predictions for biaxial cases of N_x:N_y = 5:1

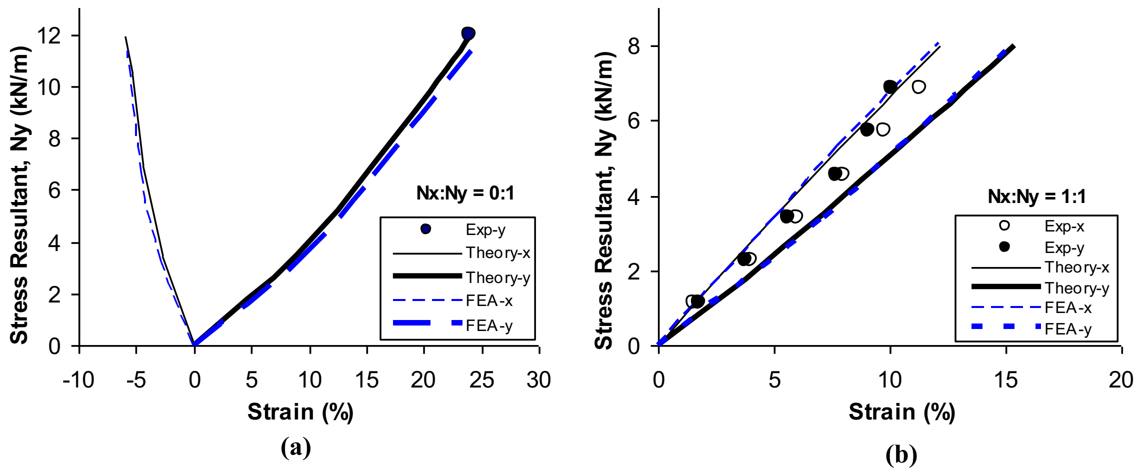

Fig. 9 Experimental data, theoretical and FEA predictions for biaxial cases of **a** N_x:N_y=0:1, and **b** N_x:N_y=1:1

the vertical axis both for filling and warp strain. The experimental data are represented by symbols, whereas the hollow circles indicate the stress–strain relationship in *x* (filling) direction and the solid circles are for *y* (warp) direction. The solid lines are the theoretical predictions based on the constitutive equations developed in this paper; whereas the thin line is for *x* (filling) direction and the thick line represents *y* (warp) direction. Similarly, the thin dash line and thick dash line are the FEA results for *x* (filling) and *y* (warp) direction, respectively. Figures 8 and 9 show the similar comparisons for the cases of N_x:N_y=0:1, 1:1, 1:2, and 1:5. Note that only the values of major loading (N_y) are used to plot in the vertical axis both for filling and warp strain. Notice that to avoid any possible singularity problem, a very small load is used instead of 0 (zero) load in the case of N_x:N_y=0:1. As indicated in the original reference, the experimental data shown in the figures are the average values with a maximum of 5% deviation from the individual data points. Considering the possible uncertainties involved, very good correlations have been found for the comparisons.

6.2 Contact forces and lateral displacements

Figure 11a shows the theoretical and FEA predictions of contact force (*P*) for the biaxial cases.

$$P = 4(F_z/2), \tag{18}$$

where $F_z/2$ is the reading of force of master node (shown in Fig. 7) along the *z* direction.

Strain in the major direction (ε_y) is used as the horizontal axis in Fig. 11a. It is clear from Fig. 10 that the contact force (*P*) is increased by the increment of minor resultant stress (N_x); as major to minor stress ratio (N_x:N_y) increases the contact force. This fabric behavior is expected because

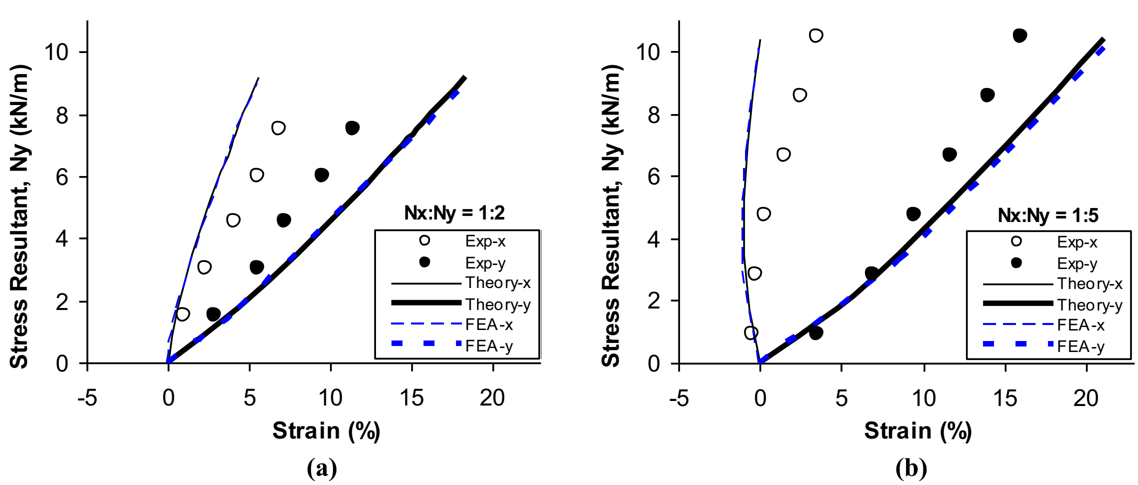

Fig. 10 Experimental data, theoretical and FEA predictions for biaxial cases of **a** N_x:N_y=1:2, and **b** N_x:N_y=1:5

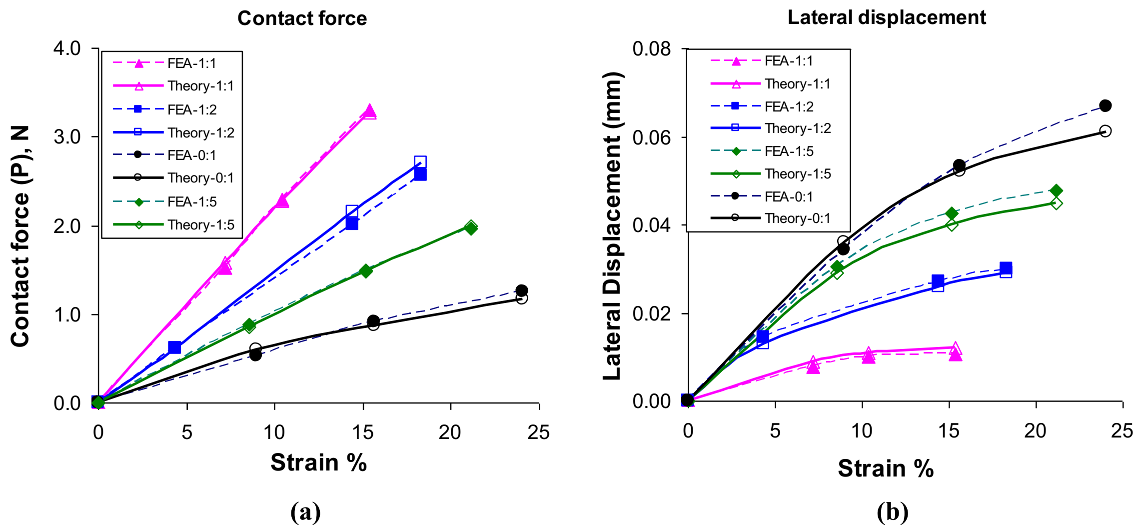

Fig. 11 Theoretical and FEA predictions for biaxial cases of **a** contact force, **b** lateral displacement (δ)

due to the increment of minor load (values of major load keep same), x-yarn and y-yarn compact each other; therefore, the contact force is increased.

Figure 11b shows the theoretical and FEA predictions of lateral displacement (δ) for the biaxial cases. It is clear from Fig. 11b that the lateral displacement (δ) is decreased by the increment of minor and major resultant stress ratio (N_x:N_y). This is the opposite behavior of contact force. This fabric behavior is expected because due to the increment of minor load, x-yarn and y-yarn compact each other; therefore, the lateral displacement is decreased.

7 Conclusions

When a plain weave fabric is subjected to biaxial loading with different loading ratios, the patterns of the nonlinear force displacement curve are significantly different. This phenomenon is caused by the fabric structure rearrangement, mainly through the crimp interchange (or the vertical displacement of the contact point between the warp and filling yarns). In this work, a sinusoidal unit cell model has been used to study the geometric nonlinearity behavior of the plain weave fabrics. All the parameters used to describe the model can be completely defined by the real physical properties of the fabric (i.e., crimps, number of yarns per unit fabric length, and yarn properties). Strain energy approach is used to establish the constitutive equation for the biaxial loading. The predictions from current model agree well with the experimental results found in the literatures for a fabric under biaxial loadings of 0:1, 1:5, 1:2, 1:1, and 5:1. They also agree well with FEA simulations of mechanical behavior of plain weave fabrics due to in-plane biaxial loading.

Acknowledgements The authors would like to thank Professor Ronald F. Gibson (University of Nevada, Reno) for valuable discussions.

Compliance with ethical standards

Conflict of interest The authors declared no potential conflicts of interest with respect to the research, authorship, and/or publication of this article.

References

Adumitroaie A, Barbero EJ (2012) Stiffness and strength prediction for plain weave textile reinforced composites. Mech Adv Mater Struct 19:169–183

Afrashteh S, Merati AA, Jeddi AAA (2013) Geometrical parameters of yarn cross-section in plain woven fabric. Indian J Fibre Text Res 38:126–131

Barbero EJ, Lonetti P, Sikkil KK (2006a) Finite element continuum damage modeling of plain weave reinforced composites. Compos B Eng 37:137–147

Barbero EJ, Trovillion J, Mayugo JA, Sikkil KK (2006b) Finite element modeling of plain weave fabrics from photomicrograph measurements. Compos Struct 73:41–52

Basit MM, Luo SY (2018) A simplified model of plain weave fabric reinforcements for the pure shear loading. Int J Mater Form 11:445–453

Behera BK, Militky J, Mishra R, Kremenakova D (2012) Modeling of woven fabrics geometry and properties. http://cdn.intechopen.com/pdfs/36900.pdf. Accessed 16 May

Boehler JP, Demmerle S, Koss S (1994) A new direct biaxial testing machine for anisotropic materials. Exp Mech 34:1–9

Boisse P, Zouari B, Daniel JL (2006) Importance of in-plane shear rigidity in finite element analyses of woven fabric composite performing. Compos A Appl Sci Manuf 37:2201–2212

Buet-Gautier K, Boisse P (2001) Experimental analysis and modeling of biaxial mechanical behavior of woven composite reinforcements. Exp Mech 41:260–269

Cao J et al (2008) Characterization of mechanical behaviour of woven fabrics: experimental methods and benchmark results. Compos A Appl Sci Manuf 39:1037–1053

Daelemans L, Faes J, Allaoui S, Hivet G, Dierick M, Hoorebeke L, Paepegem WV (2016) Finite element simulation of the woven geometry and mechanical behaviour of a 3D woven dry fabric under tensile and shear loading using the digital element method. Compos Sci Technol 137:177–187

El-Messiry M, Youssef S (2011) Analysis of stress–strain of architect woven fabric strength under biaxial extensions. Alex Eng J 50:297–303

Erol O, Powers BM, Keefe M (2017) Effects of weave architecture and mesoscale material properties on the macroscale mechanical response of advanced woven fabrics. Compos A Appl Sci Manuf 101:554–566

Freeston WD, Platt MM, Shoppe MM (1967) Mechanics of elastic performance of textile materials, part XVIII: stress strain response of fabrics under two dimensional loading. Text Res J 37:948–975

Gasser A, Boisse P, Hanklar S (2000) Mechanical behaviour of dry fabric reinforcements. 3d simulations versus biaxial tests. Comput Mater Sci 17:7–20

Ito M, Chou TW (1998) An analytical and experimental study of strength and failure behavior of plain weave composites. J Compos Mater 32:2–30

Kawabata S, Niwa M, Kawai H (1973) 3—The finite-deformation theory of plain-weave fabrics part I: the biaxial-deformation theory. J Text Inst 64:21–46

Kumazawa H, Susuki I, Morita T, Kuwabara T (2005) Mechanical properties of coated plain weave fabrics under biaxial loads. Trans Jpn Soc Aeronaut Space Sci 48:117–123

Launay J, Hivet G, Duong AV, Boisse P (2008) Experimental analysis of the influence of tensions on in plane shear behavior of woven composite reinforcements. Compos Sci Technol 68:506–515

Luo SY, Mitra A (1999) Finite elastic behavior of flexible fabric composite under biaxial loading. J Appl Mech 66:631–638

Mohammed U, Lekakou C, Dong L, Bader MG (2000) Shear deformation and micromechanics of woven fabrics. Compos A Appl Sci Manuf 31:299–308

Naik RA (1995) Failure analysis of woven and braided fabric reinforced composites. J Compos Mater 29:2334–2363

Ozgen B, Gong H (2010) Yarn geometry in woven fabrics. Text Res J 81:738–745

Page J, Wang J (2000) Prediction of shear force and an analysis of yarn slippage for a plain-weave carbon fabric in a bias extension state. Compos Sci Technol 60:977–986

Pan N (1996) Analysis of woven fabric strengths: prediction of fabric strength under uniaxial and biaxial extension. Compos Sci Technol 56:311–327

Sun H, Pan N (2005) Shear deformation analysis for woven fabrics. Compos Struct 67:317–322

Welsh JS, Adams DF (2002) An experimental investigation of the biaxial strength of IM6/3501-6 carbon/epoxy cross ply laminates using cruciform specimens. Compos A Appl Sci Manuf 33:829–839

Zhang YC, Harding J (1990) A numerical micromechanics analysis of the mechanical properties of a plain weave composite. Comput Struct 36:839–844